EDGE ARTICLE

Check for updates

Enzyme-activated near-infrared fluorogenic probe with high-efficiency intrahepatic targeting ability for visualization of drug-induced liver injury†

Yong Zhang,[ab] Xueqian Chen,[ab] Qing Yuan,[ab] Yongning Bian,[ab] Mingrui Li,[ab] Yaling Wang,[ab] Xueyun Gao [ID] *[ab] and Dongdong Su [ID] *[ab]

Hepatotoxicity is a serious problem faced by thousands of clinical drugs, and drug-induced liver injury (DILI) caused by chronic administration or overdose has become a major biosafety issue. However, the near-infrared (NIR) fluorescent probes currently used for liver injury detection still suffer from poor liver targeting ability and low sensitivity. Enzyme-activated fluorogenic probes with powerful *in situ* targeting ability are the key to improving the imaging effect of liver injury. Herein, we rationally designed a leucine aminopeptidase (LAP) activated fluorogenic probe hCy-CA-LAP, which greatly improved the hepatocyte-targeting capability by introducing a cholic acid group. The probe hCy-CA-LAP is converted into a high-emission hCy-CA fluorophore in the presence of LAP, showing high selectivity, high sensitivity and low detection limit (0.0067 U mL^{-1}) for LAP, and successfully realizes the sensitive detection of small fluctuations of LAP in living cells. Moreover, the probe can achieve effective *in situ* accumulation in the liver, thereby achieving precise imaging and evaluation of two different types of drug-induced hepatotoxicity *in vivo*. Therefore, the probe hCy-CA-LAP may be a potential tool for exploring the roles of LAP and evaluating the degree of DILI.

Introduction

As the primary metabolic organ of the human body, the liver is responsible for the biotransformation of endogenous metabolites and exogenous drugs.[1,2] Currently, more than one thousand drugs in clinical use are known to have hepatotoxicity.[3] Overdose or chronic administration of drugs has become the major safety concern in drug-induced liver injuries (DILIs), such as acute liver injury, hepatitis, fibrosis, and cholestatic liver injury.[4] For the diagnosis of DILI, the abnormal activities of alanine aminotransferase (ALT) and aspartate aminotransferase (AST) in serum are considered to be the clinical standard, but their appearance in muscle injury and kidney injury may lead to false positives in the diagnosis.[5,6] In addition, with their secretion and accumulation, when these two indicators rise to an identifiable level, patients has already suffered from severe liver disease, and has lost the opportunity for timely treatment and preventing disease progression.[7,8] With the conspicuous

advancement of imaging technology, fluorescent probes that can non-invasively visualize physiological and pathological processes at the molecular level have become an irreplaceable strategy for early and accurate diagnosis of diseases, thereby effectively preventing advanced diseases.[9–14]

Leucine aminopeptidase (LAP), widely distributed in organisms, catalyzes the crucial step in the synthesis of bioactive peptides.[15,16] In DILI, hepatic protection mechanisms help to significantly up-regulate the activity of LAP, even in the early stages.[17,18] In view of these key features, LAP is often selected as an *in situ* biomarker and specific trigger to develop activatable fluorescent probes for accurate diagnosis of DILI at an early stage.[17,19,20] Compared with always-on probes, activatable fluorogenic probes with high selectivity and low background signal provide a high signal-to-background ratio (SBR) when detecting biomarkers of interest.[21–25] At the same time, in order to reduce organic autofluorescence and scattering, and improve the sensitivity, NIR probes facilitate *in vivo* high SBR imaging, because they have numerous advantages such as minimum photodamage to biological samples, low interference from tissue autofluorescence and deeper signal feedback depth.[26–29] He *et al.* successfully reported an activatable NIR fluorogenic probe for high contrast *in situ* imaging of LAP activity in a DILI mouse model.[30] Yuan *et al.* screened and designed two chemically stable activatable NIR fluorogenic probes for *in vivo* imaging of DILI-related biomarkers (LAP and ONOO⁻), and visually evaluated the therapeutic effects of clinical

[a]Department of Chemistry and Biology, Faculty of Environment and Life Science, Beijing University of Technology, Beijing, 100124, P. R. China. E-mail: chmsudd@bjut.edu.cn; gaoxy@ihep.ac.cn

[b]Center of Excellence for Environmental Safety and Biological Effects, Beijing University of Technology, Beijing, 100124, P. R. China

† Electronic supplementary information (ESI) available: Experimental details, synthesis and characterization data, and additional spectra and imaging data. See DOI: 10.1039/d1sc04825b

hepatoprotective drugs.[31] Wang *et al.* designed LAP-activated fluorescent probes based on intramolecular rearrangement for high SBR detection of LAP in living systems.[32,33]

Although the currently reported probes provide the primary merits of high selectivity, real-time feedback and tailor-made features, small molecular fluorogenic probes for visualization of drug-induced liver injury still have obvious disadvantages.[11,34,35] Most imaging probes enter the liver through passive targeting and suffer from rapid clearance in the liver, which makes it difficult for those probes to accumulate adequately inside the liver within a short time, resulting in low signal strength and sensitivity in the liver region.[36,37] Active targeting strategies can significantly improve the accumulation of small molecular probes in the region of interest by introducing functional groups.[27,38–41] Therefore, it is highly desirable to design probes with stronger intrahepatic targeting capability to improve the *in situ* accumulation and imaging sensitivity of the probe in the liver, which can apparently facilitate the diagnosis of DILI as well as further research on the clinical biological characteristics of biomarkers. As a signalling molecule, cholic acid is involved in multiple pathways in the liver, and can be actively transported into hepatocytes, showing inherent hepatocyte targeting.[42–44] In view of the key features, a few dyes and prodrugs modified with cholic acid have been designed to enhance their *in situ* delivery in the liver.[36,45,46] Therefore, cholic acid can serve as a potential group to develop probes with efficient hepatic targeting ability.

In this work, we report a cholic acid-modified NIR fluorogenic probe (**hCy-CA-LAP**) for fluorescence imaging of DILI. The introduction of cholic acid can improve the intrahepatic targeting capability of **hCy-CA-LAP**, thereby significantly increasing the enrichment of probe molecules in the liver.[36,47] **hCy-CA-LAP** is composed of an NIR fluorescence signaling moiety (hemicyanine fluorophore, **hCy**), a hepatocyte-targeting moiety (cholic acid) for efficient hepatic enrichment, and a LAP recognition moiety (L-leucine amide). The recognition part is connected to the fluorophore **hCy-CA** through a self-immolative linker, and serves as the LAP-responsive part and fluorescence quencher (Scheme 1). The probe **hCy-CA-LAP** can achieve effective *in situ* accumulation in the liver, where it is converted into a high-emission **hCy-CA** fluorophore by the pathological level of LAP in DILI. The combination of activatability, NIR

fluorescence and highly targeted accumulation can effectively improve the *in vivo* imaging effect and realize the highly sensitive and intensive diagnosis of DILI in the early stage.

Results and discussion

Design and synthesis of hCy-CA-LAP and hCy-LAP

Here, we designed an NIR fluorogenic probe **hCy-CA-LAP** with efficient intrahepatic targeting and LAP response characteristics. The **hCy** skeleton was chosen as the signal reporter because of its strong NIR fluorescence and multiple modifiable sites for introducing the targeting group and analyte response group.[35] **hCy-NH$_2$** was synthesized according to the reported method.[48] First, the intrahepatic targeting group cholic acid was incorporated into the fluorophore to obtain **hCy-CA**, which is the precursor of the probe **hCy-CA-LAP**. **hCy-CA** consists of a hydroxyl group at the end of the NIR fluorophore, which is the reason for its high quantum yield. Subsequently, Fmoc-Leu-Br was introduced into the precursor through a nucleophilic substitution reaction, and finally the probe **hCy-CA-LAP** was obtained after Fmoc deprotection, which we hoped would give rise to a fluorogenic LAP-reactive probe (Scheme S1†). The reduction in the fluorescence of the probe **hCy-CA-LAP** is attributed to the intramolecular photoinduced electron transfer (PeT) process from the excited fluorophore to the free amine. As a prediction, upon incubation with LAP, L-leucine amide in **hCy-CA-LAP** will be eliminated by the hydrolysis of LAP, and then a 1,6-elimination of the self-immolative linker will lead to the regeneration of free **hCy-CA**, leading to fluorescence recovery. At the same time, **hCy-LAP** without the hepatocyte-targeting moiety was constructed as a control probe. All chemical structures are fully characterized by nuclear magnetic resonance
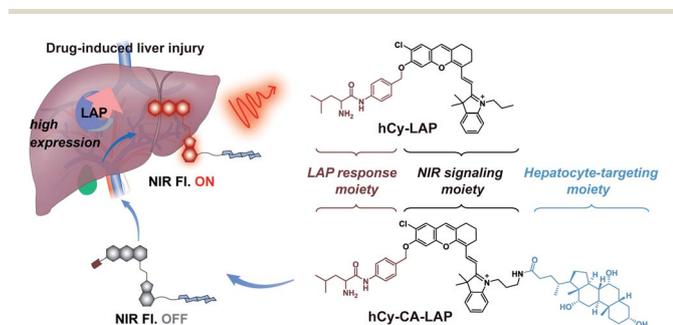
Scheme 1 Chemical structures of **hCy-CA-LAP** and **hCy-LAP**, and schematic illustration of **hCy-CA-LAP** for fluorescence imaging of LAP in DILI.
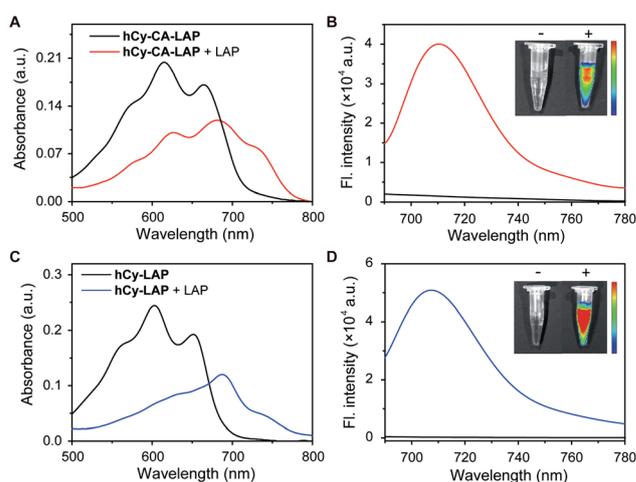

Fig. 1 *In vitro* response of **hCy-CA-LAP** and **hCy-LAP** toward LAP. Absorption spectra and fluorescence spectra of **hCy-CA-LAP** (A and B) and **hCy-LAP** (C and D) (10 μM) in the absence and presence of LAP (0.2 U mL^{-1}), λ_{ex} = 680 nm. (Insets B and D) NIR fluorescence images of the two probes before and after reacting with LAP, λ_{ex} = 640 nm and λ_{em} = 740 nm. All spectra were recorded in PBS buffer (10 mM, pH = 7.4, containing 1% DMSO) at 37 °C.

(NMR) and high-resolution electrospray ionization mass spectrometry (HRMS-ESI), as shown in the ESI (Fig. S15–S22†).

Selective detection of LAP *in vitro*

The optical properties of the two probes and their responsiveness to LAP were evaluated. As shown in Fig. 1, **hCy-CA-LAP** and **hCy-LAP** had maximum absorption peaks at 615 nm and 603 nm and negligible fluorescence intensity due to the quenching effect of the free amine in the reactive group ($\Phi < 0.01$). After reacting with LAP, the maximum absorption peaks of both probes produced a bathochromic shift to about 680 nm. The fluorescence intensity of **hCy-CA-LAP** at 710 nm dramatically increased by 27 times ($\Phi = 0.20$) compared with that of **hCy-CA-LAP** alone. Under the same conditions, the fluorescence intensity of the control probe **hCy-LAP** at 705 nm increased by 78-times ($\Phi = 0.27$) in response to LAP stimulation (Table S1†). The NIR fluorescence images of both probes also showed high-contrast fluorescence changes, with no fluorescence in the probe-only sample and significantly increased fluorescence in the LAP-treated sample (Fig. 1B and D inner images). This indicates that both probes are converted into high emission fluorophores with high SBR fluorescence in the NIR region, which shows favorable sensitivity to LAP. Meanwhile, the maximum fluorescence peaks of the two probes differ by 5 nm. It is speculated that the introduction of the hydrophobic cholic acid group weakens the water solubility of the probe **hCy-CA-LAP**, which is related to the affinity to LAP and optical performance in aqueous solution. In addition, **hCy-CA-LAP**, **hCy-LAP** and their products displayed satisfactory photostability after 3 hours of continuous irradiation, suggesting the possibility of using them as LAP-activated NIR probes (Fig. S1†).

A more detailed *in vitro* selective detection of LAP was performed. As shown in Fig. 2A, the time curve of the fluorescence intensity of **hCy-CA-LAP** and different concentrations of LAP at 710 nm showed that the reaction reached a plateau within 1 h. Under the same conditions, the fluorescence intensity of **hCy-LAP** at 705 nm reached a plateau in about 40 min (Fig. S2A†). Taking into account the difference in response equilibrium times of the two probes, the incubation time was 60 min for **hCy-CA-LAP** and 40 min for **hCy-LAP** throughout the *in vitro* experiment. The fluorescence changes of **hCy-CA-LAP** in the presence of different concentrations of LAP are presented in Fig. 2B. A higher concentration of LAP can promote the reaction with **hCy-CA-LAP** and the release of the fluorophore. At the same time, the fluorescence intensity of **hCy-CA-LAP** at 710 nm gradually increased with incremental concentrations of LAP, and reached a basic equilibrium when the LAP concentration was 0.075 U mL^{-1}, and exhibited good linearity at low concentrations of LAP (0–0.075U mL^{-1}) (Fig. 2C and D). A similar trend in fluorescence response to different concentrations of LAP was also observed when testing **hCy-LAP** (Fig. S2†). The limit of detection (LOD) of **hCy-CA-LAP** and **hCy-LAP** was determined to be 0.0067 U mL^{-1} and 0.002 U mL^{-1} calculated using the formula $3\sigma/k$, respectively (Table S1†). Therefore, **hCy-CA-LAP** and **hCy-LAP** are capable of well quantifying the content and activity of LAP based on the changes in fluorescence.

High-performance liquid chromatography (HPLC) and HRMS-ESI were used to further verify the above reaction mechanism. HPLC results showed that probe **hCy-CA-LAP** had a clear characteristic peak at 5.341 min. After the addition of LAP, the probe peak decreased significantly and a new peak appeared (retention time, TR = 6.048 min), which was the same
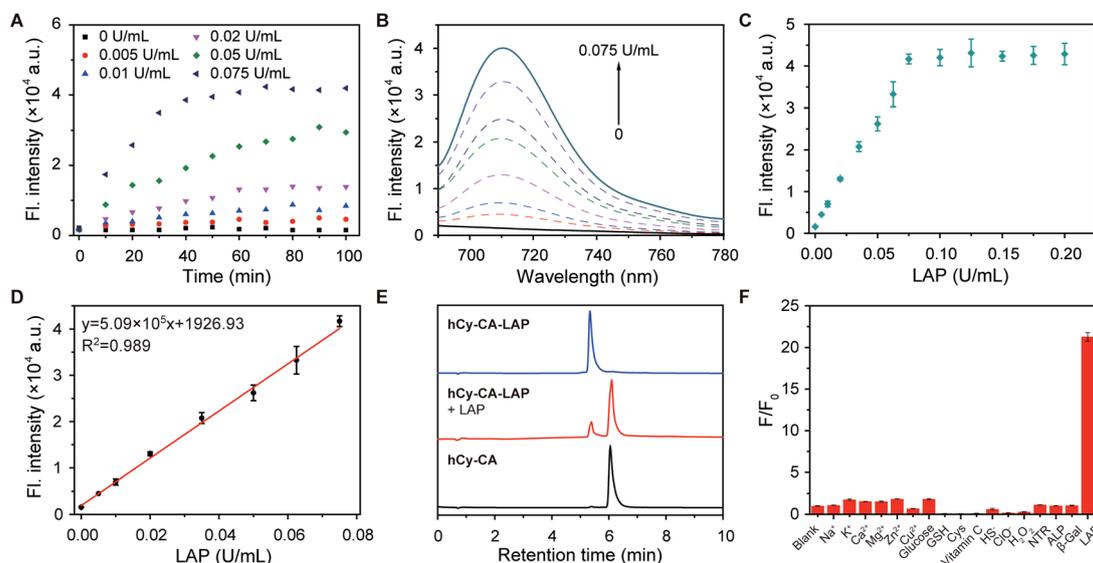

Fig. 2 *In vitro* response of **hCy-CA-LAP** toward LAP. (A) The sensing kinetics of **hCy-CA-LAP** ($F_{710\ nm}$) and (B) fluorescence responses of **hCy-LAP** (10 μM) to different concentrations of LAP (0–0.075 U mL^{-1}). (C) Fluorescence intensity of **hCy-CA-LAP** (10 μM) at 710 nm with different concentrations of LAP (0–0.2 U mL^{-1}). (D) Linear correlation between the fluorescence intensity of **hCy-CA-LAP** at 710 nm and low concentrations of LAP (0–0.075 U mL^{-1}). (E) Chromatograms of **hCy-CA-LAP**, **hCy-CA-LAP** reacting with LAP and **hCy-CA**, $\lambda_{abs} = 600$ nm. (F) Fluorescence response of **hCy-CA-LAP** (10 μM) to different analytes (analytes: 1 mM, enzyme: 0.1 U mL^{-1}) in PBS buffer (pH 7.4) at 37 °C. $\lambda_{ex} = 680$ nm, $\lambda_{em} = 705$ nm.

as that of the product **hCy-CA** (Fig. 2E). Synchronous mass spectrometry further confirmed the results. The mass spectrum clearly showed the characteristic peak of **hCy-CA-LAP** with a molecular weight of $m/z = 1069.6185$ $[M]^+$ (calculated $m/z = 1069.6180$ $[M]^+$) (Fig. S3†). After treating with LAP, a new mass peak appeared at $m/z = 851.4788$ $[M]^+$, which was consistent with the expected product **hCy-CA** (calculated $m/z = 851.4760$, $[M]^+$) (Fig. S4†). This is strong evidence confirming the successful release of **hCy-CA** by the LAP-catalyzed elimination of the L-leucine amide moiety and the spontaneous elimination of the self-immolative linker, which is consistent with the expected reaction mechanism. HPLC and HRMS-ESI data also demonstrated the successful release of **hCy** (TR = 5.975 min, $m/z = 446.1889$ $[M]^+$) from **hCy-LAP** (TR = 5.300 min, $m/z = 664.3382$ $[M]^+$) after incubating with LAP (Fig. S5–S7†).

Subsequently, to demonstrate the potential for unique recognition of LAP, the selectivity of the LAP-activated probe in the presence of other potential coexisting interferents was evaluated, including ions (Na^+, K^+, Ca^{2+}, Mg^{2+}, Zn^{2+}, Cu^{2+}), biomolecules (glucose, glutathione, cysteine, vitamin C), redox species (HS^-, ClO^-, H_2O_2) and related enzymes (nitroreductase, alkaline phosphatase, β-galactosidase). The results showed that fluorescence intensity was negligible after incubation of **hCy-CA-LAP** or **hCy-LAP** with those potential interferents (Fig. 2F and S8†). Both **hCy-CA-LAP** and **hCy-LAP** can react rapidly with the individual enzyme LAP, with a strong fluorescence enhancement, rather than with other potential interference species. In addition, a change in pH from 5.0 to 9.0 had little effect on the response of the two probes to LAP, indicating that both probes performed well under physiological conditions (Fig. S9†). Therefore, they can serve as effective probes for selective detection of LAP under complex physiological conditions.

Fluorescence imaging of endogenous LAP in living cells

Inspired by the outstanding performance *in vitro*, we evaluated the potential of these two probes to monitor endogenous LAP in living cells. The biocompatibility of the probe was evaluated by exposing LO2 or HepG2 cells to various concentrations of **hCy-CA-LAP** or **hCy-LAP** for 24 h, respectively. As shown in Fig. S10,† more than 95% of LO2 and HepG2 cells survived even at 10 μM **hCy-CA-LAP**, indicating that the cytotoxicity of **hCy-CA-LAP** to living cells was negligible. To our surprise, for the control probe, 10 μM **hCy-LAP** significantly reduced the cell viability, where the viability of LO2 cells was 47% and that of HepG2 cells was only 34%. Therefore, only **hCy-CA-LAP** with good biocompatibility was further used to detect and monitor endogenous LAP in LO2 and HepG2 cells.

Acetaminophen (APAP) treatment at a toxic dosage has been proved to induce hepatocyte injury, accompanied by a complex cascade of hepatic self-protection pathways.[49,50] Several experiments have reported that the up-regulation of LAP is a biomarker that is significantly related to hepatocyte injury.[51–53] Therefore, we tested the activity level of LAP in cells stimulated by drugs. As shown in Fig. 3A and C, the fluorescence of LO2 cells was weak after treatment with **hCy-CA-LAP**, which is due to the relatively low concentration of LAP in normal LO2 cells under physiological conditions. To manifest the specificity of the probe, bestatin, an activity inhibitor of LAP, was used in further study.[54] After pretreatment with bestatin for 1 h, the LO2 cells incubated with **hCy-CA-LAP** had almost no fluorescence. Compared with the control group without bestatin, the
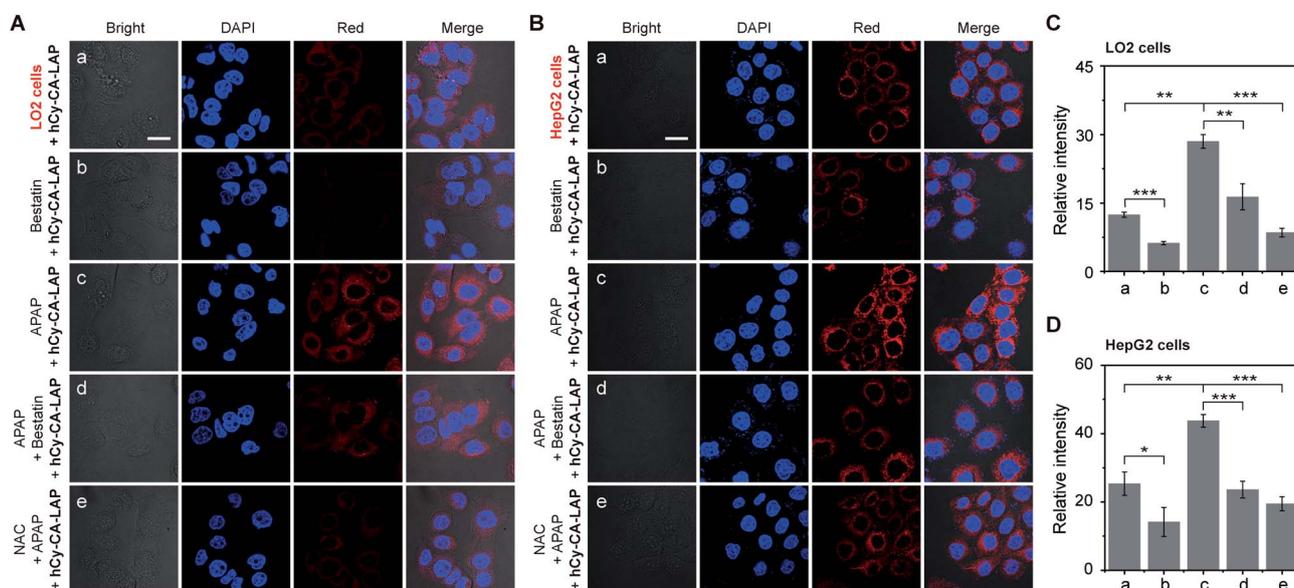

Fig. 3 Fluorescence imaging of LO2 cells (A) and HepG2 cells (B) incubated with **hCy-CA-LAP** (10 μM) for 30 min: (a) untreated cells; (b) cells pretreated with 100 μM bestatin for 1 h; (c) cells pretreated with 1 mM APAP for 12 h; (d) cells pretreated with 1 mM APAP for 12 h, and then treated with 100 μM bestatin for 1 h; (e) cells pretreated with 100 μM NAC for 1 h, and then treated with 1 mM APAP for 12 h. (C) and (D) Relative fluorescence intensity of the corresponding fluorescence images in panels A and B, $\lambda_{ex} = 639$ nm, $\lambda_{em} = 663–738$ nm. Scale bar: 25 μm. *$P < 0.05$, **$P < 0.01$, and ***$P < 0.001$.

significantly suppressed fluorescence intensity proved that the fluorescence response of **hCy-CA-LAP** in cells was closely related to the enzymatic activity of LAP. In the APAP stimulation group, the fluorescence of LO2 cells increased significantly after 12 h of APAP pretreatment, while the fluorescence of the APAP + bestatin + **hCy-CA-LAP** group was significantly suppressed compared with the group treated with APAP only. After that, the protective effect of *N*-acetylcysteine (NAC), a hepatic protectant used to repair APAP-induced hepatocyte injury, was tested.[31] The results showed that NAC pretreatment also significantly suppressed the fluorescence intensity. A similar trend in fluorescence changes after incubation with **hCy-CA-LAP** was also observed in HepG2 cells (Fig. 3B and D). Therefore, the release of free **hCy-CA** and the unique fluorescence response of **hCy-CA-LAP** are indeed caused by the specific cleavage by LAP in cells. As a further proof of the concept, a comparison of fluorescence intensity was observed in two cell lines with different LAP enzyme activities. Compared with LO2 cells with a physiological level of LAP activity, after treatment with **hCy-CA-LAP**, brighter fluorescence was observed in HepG2 cells with highly expressed LAP. Therefore, this dramatically fluctuant fluorescence intensity was closely related to the activity and content of LAP in cells, proving that **hCy-CA-LAP** had excellent selectivity and sensitivity for imaging endogenous LAP in living cells.

Fluorescence imaging of LAP in a mouse model of APAP-induced acute liver injury

Acute liver injury may occur in healthy individuals without a history of related diseases or in patients who have already suffered from serious diseases.[55] If left untreated, DILI can develop into severe damage.[56,57] It is very important to develop intrahepatic targeted molecular probes for accurate diagnosis of acute liver injury *in vivo*. Although the probe **hCy-LAP** has shown toxicity to LO2 cells in previous cell experiments, *in vivo* imaging of **hCy-LAP** can still be used as a control probe to observe whether the additional cholic acid has a beneficial effect on imaging performance *in vivo*. Balb/c female mice were intraperitoneally injected with an overdose of APAP (300 mg kg^{-1}) for 1 h as the model of acute liver injury, and mice injected with an equal volume of PBS solution were used as a control group. All mice were then injected intravenously with **hCy-CA-LAP** or **hCy-LAP** (50 μM, 100 μL) for *in vivo* fluorescence imaging (Fig. 4A). As shown in Fig. 4B and C, after the administration of **hCy-CA-LAP**, the fluorescence signal in the liver region gradually increased over time, indicating the rapid intrahepatic accumulation of **hCy-CA-LAP** and its rapid response to intrahepatic LAP. Throughout the imaging process, significantly higher fluorescence signals were observed in APAP-
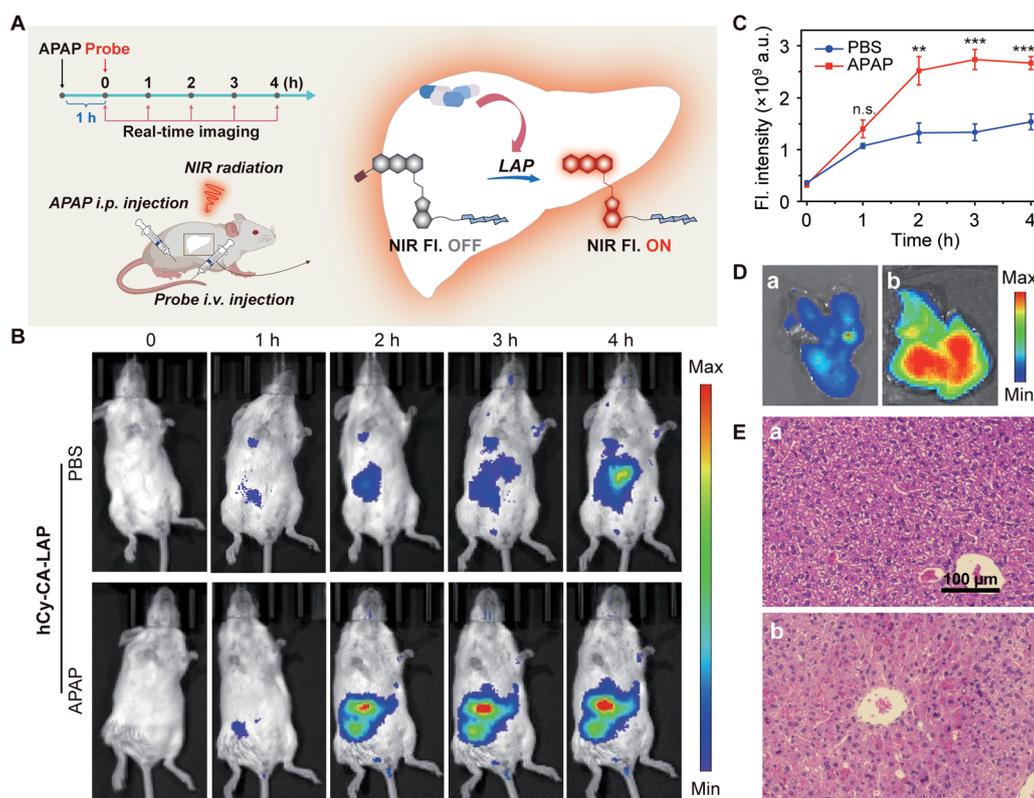

Fig. 4 *In vivo* fluorescence imaging of APAP-induced acute liver injury. (A) Schematic diagram of APAP-induced acute liver injury mouse model construction and *in vivo* fluorescence imaging of LAP. (B) Time-dependent *in vivo* fluorescence imaging. Balb/c female mice were pretreated with APAP (300 mg kg^{-1}, 200 μL) or PBS (200 μL) for 1 h, and then injected intravenously with **hCy-CA-LAP** (50 μM, 100 μL). (C) Quantification of the fluorescence signal in (B) **$P < 0.01$, and ***$P < 0.001$, and n.s.: not significant, compared with the control group (PBS-treated group). (D) *Ex vivo* imaging of liver dissected from mice after intravenously injected with **hCy-CA-LAP** (50 μM, 100 μL) for 3 h. (E) Histological study of liver tissues from Balb/c mice treated with APAP (300 mg kg^{-1}, 200 μL) and PBS (200 μL), $\lambda_{ex} = 640$ nm, $\lambda_{em} = 740$ nm.

stimulated mice compared to the control group, achieving high-performance *in vivo* imaging of DILI with high sensitivity. The fluorescence intensity of the dissected liver which was administered **hCy-CA-LAP** showed a more significant increase between APAP and PBS-treated mice (Fig. 4D). The *in vivo* biodistribution of **hCy-CA-LAP** indicated that the probe was mainly distributed in the liver (Fig. S11†). Moreover, the liver tissues stained with hematoxylin & eosin (H&E) were also analyzed to evaluate liver injury. There was no obvious morphological change in the liver tissue of PBS-treated mice, while swollen hepatocytes and Kupffer cell proliferation were observed in that of APAP-treated mice (Fig. 4E). In addition, mice treated with APAP and PBS injected intravenously with **hCy-LAP** showed a similar trend of fluorescence change to **hCy-CA-LAP** (Fig. S12†). However, in contrast to the faster response and better performance of **hCy-LAP** than **hCy-CA-LAP** throughout the *in vitro* test, when applied to *in vivo* fluorescence imaging of DILI mice, the enriched imaging of the probe **hCy-CA-LAP** in the liver showed stronger fluorescence and higher hepatic targeting ability than **hCy-LAP** under the same APAP administration conditions. Although **hCy-LAP** showed a relatively stronger fluorescence signal in DILI mice than normal mice, further quantitative data showed that **hCy-CA-LAP** had a significantly stronger imaging signal at the

liver site than **hCy-LAP** (Fig. S13†). *In vivo* results showed that the additional cholic acid group in the structure of **hCy-CA-LAP** as an intrahepatic targeting moiety can increase the enrichment of probe molecules in the liver, which will significantly improve the imaging sensitivity in the liver. Therefore, this design provides a promising strategy for effective intrahepatic targets of *in vivo* imaging probes and prodrugs.

Fluorescence imaging of LAP in a mouse model of RFP-induced cholestatic liver injury

Rifampicin (RFP) is a first-line oral agent for the treatment of tuberculosis.[58] However, hepatotoxicity is a well-known side effect of improper use of RFP, which poses a risk to patients who take RFP for a long period.[59] Biliary excretion disorder is the primary pathological symptom caused by long-term use of RFP. If left untreated, it can develop into cholestatic liver injury cirrhosis.[60] Therefore, it is of great significance to develop highly sensitive and accurate methods for early detection of cholestatic liver injury.

Our aim was to image and map the enzymatic activity of LAP in a mouse model of cholestatic liver injury. Cholestatic liver injury leads to an elevated activity of intrahepatic LAP. In this
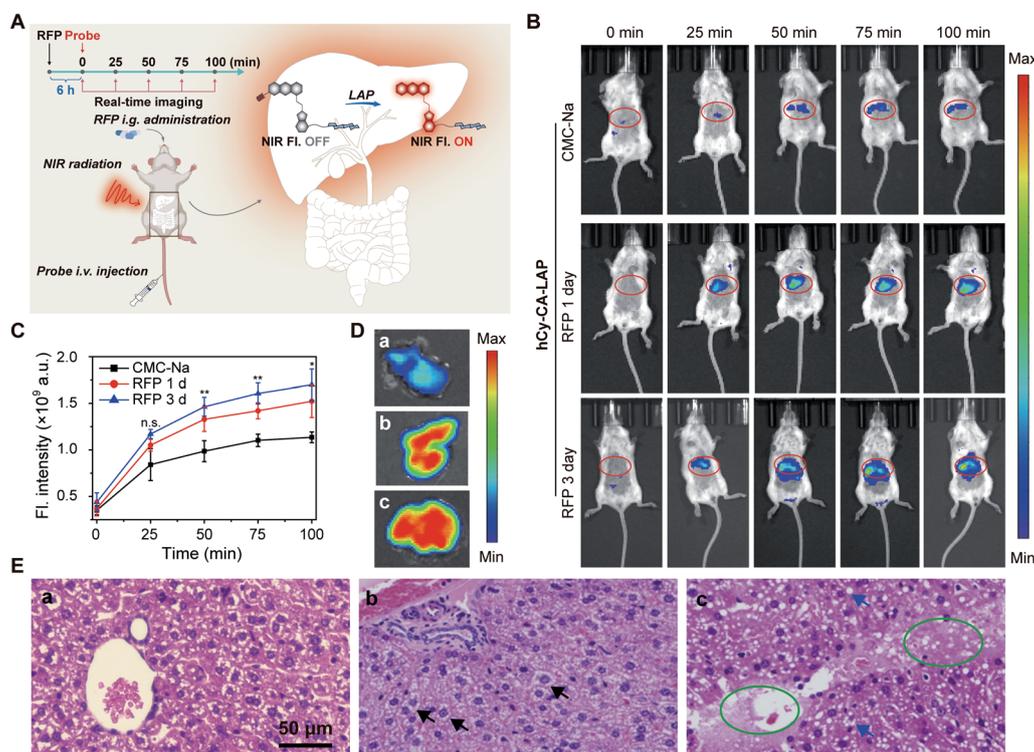

Fig. 5 *In vivo* fluorescence imaging of RFP-induced cholestatic liver injury. (A) Schematic diagram of **hCy-CA-LAP** for fluorescence imaging of LAP in a mouse model of RFP-induced cholestatic liver injury. (B) Time-dependent *in vivo* fluorescence imaging. Balb/c female mice were given RFP (300 mg kg^{-1} d^{-1}, dissolved in 200 μL aqueous solution of 0.5% CMC-Na) intragastrically for 1 or 3 days, and RFP-free CMC-Na aqueous solution (200 μL) was intragastrically given as control, and then intravenously injected with **hCy-CA-LAP** (50 μM, 100 μL) at 6 h after the last drug treatment. $\lambda_{ex} = 640$ nm, $\lambda_{em} = 740$ nm. (C) Quantification of fluorescence signal in (B). *$P < 0.05$, and **$P < 0.01$, and n.s.: not significant, compared with the control group (CMC-Na treated group). (D) *Ex vivo* imaging of livers dissected from mice after intravenously injected with **hCy-CA-LAP** for 60 min. (E) Histology studies of liver tissues from Balb/c mice treated with RFP for 1 or 3 days and CMC-Na solution. Black arrows: swollen hepatocytes; blue arrows: lipid vacuoles; green circles: nuclear debris and necrosis of hepatocytes.

experiment, untreated female Balb/c mice were randomly divided into three groups. After fasting overnight, the mice were given RFP intragastrically at a hepatotoxic dosage (300 mg kg^{-1} d^{-1}) for one or three days. The control group was given carboxymethylcellulose sodium (CMC-Na) solution (200 μL) intragastrically. **hCy-CA-LAP** was then intravenously administered 6 h after the last drug treatment (Fig. 5A). Initially, there was no fluorescence signal in the abdomen of the mice receiving a single dose of RFP, but over time, the fluorescence signal in the upper abdomen gradually increased and matched well with the liver region, indicating elevated intrahepatic LAP levels (Fig. 5B). Compared with the single-dose RFP group, a higher fluorescence signal was observed in the upper abdomen of mice treated with 3 times the dose of RFP. In contrast, obviously weak fluorescence was observed throughout the imaging process in the CMC-Na-treated group. Similarly, the quantitative signal also showed a higher fluorescence signal than the CMC-Na-treated group for imaging RFP-induced cholestatic liver injury, indicating that the probe **hCy-CA-LAP** with an intrahepatic target can map the hepatic LAP level (Fig. 5C). The fluorescence intensity of the dissected liver which was administered **hCy-CA-LAP** showed significant differences between mice treated with RFP for one or three days and control mice (Fig. 5D). The histological analysis of liver tissue was also conducted to evaluate liver injury. There were no obvious pathological changes in the CMC-Na-treated group, indicating that 5% CMC-Na aqueous solution has no hepatotoxicity. In contrast, swollen hepatocytes were observed in mice that received a single dose of RFP. In addition to the swollen hepatocytes, more obvious pathological changes such as lipid vacuoles, cholestasis, nuclear debris and hepatocyte necrosis indicated that the liver injury in mice treated with 3 times the dose of RFP was more severe (Fig. 5E). The *in vivo* biodistribution of **hCy-CA-LAP** showed that the probe was mainly distributed in the liver (Fig. S14†). Due to its excellent imaging features, **hCy-CA-LAP** can serve as an effective strategy for early and accurate diagnosis of RFP-induced cholestatic liver injury and in further research on the clinical biological characteristics of biomarkers.

Conclusions

In summary, we have constructed a LAP-activated NIR fluorogenic probe with high hepatocyte-targeting ability for accurate and sensitive imaging of LAP in DILI. Probe **hCy-CA-LAP** provided a low detection limit for LAP (0.0067 U mL^{-1}) and achieved sensitive detection of small fluctuations of LAP in living cells. The introduction of cholic acid realized the high-efficiency intrahepatic targeting of **hCy-CA-LAP**, which contributed to the highly sensitive and high-contrast imaging of LAP *in vivo*. Furthermore, **hCy-CA-LAP** further demonstrated the ability to visualize the pathological level of LAP in the mouse model of APAP or RFP induced liver injury. Therefore, our work may provide an effective strategy for facilitating DILI diagnosis, medicine evaluation and further research on the clinical and biological characteristics of biomarkers.

Data availability

Primary data for probe synthesis, characterization, photophysical measurements, and fluorescence imaging data are provided in the ESI.†

Author contributions

D. S., X. G. designed, supervised and analyzed the experiments. Y. Z., X. C. and Q. Y. contributed to the initial implementation, data analysis and manuscript preparation. Y. B., M. L. and Y. W. contributed to the synthesis and characterization. The manuscript was written through the contributions of all authors. All authors have given approval to the final version of the manuscript.

Conflicts of interest

There are no conflicts to declare.

Acknowledgements

Notes and references

1 D. E. Williams, R. L. Reed, B. Kedzierski, G. A. Dannan, F. P. Guengerich and D. R. Buhler, *Drug Metab. Dispos.*, 1989, **17**, 387–392.

2 J. Chen, D. Huang, M. She, Z. Wang, X. Chen, P. Liu, S. Zhang and J. Li, *ACS Sens.*, 2021, **6**, 628–640.

3 A. Pandit, T. Sachdeva and P. Bafna, *J. Appl. Pharm. Sci.*, 2012, **2**, 233–243.

4 C. Y. Chang and T. D. Schiano, *Aliment. Pharmacol. Ther.*, 2007, **25**, 1135–1151.

5 J. Peng, A. Samanta, X. Zeng, S. Han, L. Wang, D. Su, D. T. Loong, N. Y. Kang, S. J. Park, A. H. All, W. Jiang, L. Yuan, X. Liu and Y. T. Chang, *Angew. Chem., Int. Ed.*, 2017, **56**, 4165–4169.

6 R. A. Nathwani, S. Pais, T. B. Reynolds and N. Kaplowitz, *Hepatology*, 2005, **41**, 380–382.

7 M. C. Kew, *Lancet*, 2000, **355**, 591–592.

8 D. Cheng, W. Xu, X. Gong, L. Yuan and X. B. Zhang, *Acc. Chem. Res.*, 2021, **54**, 403–415.

9 X. Chen, Y. Bian, M. Li, Y. Zhang, X. Gao and D. Su, *Chem.–Asian J.*, 2020, **15**, 3983–3994.

10 D. Su, X. Chen, Y. Zhang and X. Gao, *TrAC, Trends Anal. Chem.*, 2020, **133**, 116112.

11 H. W. Liu, L. Chen, C. Xu, Z. Li, H. Zhang, X. B. Zhang and W. Tan, *Chem. Soc. Rev.*, 2018, **47**, 7140–7180.

12 H. Xiao, C. Wu, P. Li, W. Gao, W. Zhang, W. Zhang, L. Tong and B. Tang, *Chem. Sci.*, 2017, **8**, 7025–7030.

13 X. Ai, Z. Wang, H. Cheong, Y. Wang, R. Zhang, J. Lin, Y. Zheng, M. Gao and B. Xing, *Nat. Commun.*, 2019, **10**, 1087.

14 P. Cheng, Q. Miao, J. Huang, J. Li and K. Pu, *Anal. Chem.*, 2020, **92**, 6166–6172.

15 M. Matsui, J. H. Fowler and L. L. Walling, *Biol. Chem.*, 2006, **387**, 1535–1544.

16 M. Tsujimoto, Y. Goto, M. Maruyama and A. Hattori, *Heart Fail. Rev.*, 2008, **13**, 285–291.

17 Y. Huang, Y. Qi, C. Zhan, F. Zeng and S. Wu, *Anal. Chem.*, 2019, **91**, 8085–8092.

18 J. R. Senior, *Clin. Pharmacol. Ther.*, 2012, **92**, 332–339.

19 Y. Liu, L. Teng, C. Xu, H. W. Liu, S. Xu, H. Guo, L. Yuan and X. B. Zhang, *Chem. Sci.*, 2019, **10**, 10931–10936.

20 T. Liu, M. Tian, J. Wang, X. Tian, J. Liu, L. Feng, X. Ma and J. Cui, *Spectrochim. Acta, Part A*, 2021, **251**, 119362.

21 A. Razgulin, N. Ma and J. Rao, *Chem. Soc. Rev.*, 2011, **40**, 4186–4216.

22 P. Zhang, X.-f. Jiang, X. Nie, Y. Huang, F. Zeng, X. Xia and S. Wu, *Biomaterials*, 2016, **80**, 46–56.

23 W. Zhang, J. Liu, P. Li, X. Wang, S. Bi, J. Zhang, W. Zhang, H. Wang and B. Tang, *Biomaterials*, 2019, **225**, 119499.

24 Z. Wang, X. Ai, Z. Zhang, Y. Wang, X. Wu, R. Haindl, E. K. L. Yeow, W. Drexler, M. Gao and B. Xing, *Chem. Sci.*, 2019, **11**, 803–811.

25 L. Wu, J. Huang, K. Pu and T. D. James, *Nat. Rev. Chem.*, 2021, **5**, 406–421.

26 J. Ou-Yang, Y. Li, W. L. Jiang, S. Y. He, H. W. Liu and C. Y. Li, *Anal. Chem.*, 2019, **91**, 1056–1063.

27 M. Gao, F. Yu, C. Lv, J. Choo and L. Chen, *Chem. Soc. Rev.*, 2017, **46**, 2237–2271.

28 H.-W. Liu, L. Chen, C. Xu, Z. Li, H. Zhang, X.-B. Zhang and W. Tan, *Chem. Soc. Rev.*, 2018, **47**, 7140–7180.

29 Z. Lei, C. Sun, P. Pei, S. Wang, D. Li, X. Zhang and F. Zhang, *Angew. Chem., Int. Ed.*, 2019, **58**, 8166–8171.

30 X. He, L. Li, Y. Fang, W. Shi, X. Li and H. Ma, *Chem. Sci.*, 2017, **8**, 3479–3483.

31 D. Cheng, J. Peng, Y. Lv, D. Su, D. Liu, M. Chen, L. Yuan and X. Zhang, *J. Am. Chem. Soc.*, 2019, **141**, 6352–6361.

32 T. Wang, Q. Sun, H. Xiong, C. Ma, C. Lu, J. Nie, G. Yang, Z. Chen, Y. Zhang, J. Ren, F. Wang and W.-H. Zhu, *Sens. Actuators, B*, 2020, **321**, 128631.

33 Z. Zhou, F. Wang, G. Yang, C. Lu, J. Nie, Z. Chen, J. Ren, Q. Sun, C. Zhao and W. H. Zhu, *Anal. Chem.*, 2017, **89**, 11576–11582.

34 R. Yan, Y. Hu, F. Liu, S. Wei, D. Fang, A. J. Shuhendler, H. Liu, H. Y. Chen and D. Ye, *J. Am. Chem. Soc.*, 2019, **141**, 10331–10341.

35 Z. Huang, R. An, S. Wei, J. Wang and D. Ye, *Analyst*, 2021, **146**, 1865–1871.

36 Y. Wu, S. Huang, J. Wang, L. Sun, F. Zeng and S. Wu, *Nat. Commun.*, 2018, **9**, 3983.

37 D.-Q. Wu, B. Lu, C. Chang, C.-S. Chen, T. Wang, Y.-Y. Zhang, S.-X. Cheng, X.-J. Jiang, X.-Z. Zhang and R.-X. Zhuo, *Biomaterials*, 2009, **30**, 1363–1371.

38 X. Chen, Y. Zhang, Q. Yuan, M. Li, Y. Bian, D. Su and X. Gao, *J. Mater. Chem. B*, 2021, **9**, 6614–6622.

39 P. Gao, W. Pan, N. Li and B. Tang, *Chem. Sci.*, 2019, **10**, 6035–6071.

40 N. Choi, S.-M. Kim, K. S. Hong, G. Cho, J.-H. Cho, C. Lee and E. K. Ryu, *Biomaterials*, 2011, **32**, 7151–7158.

41 H. Wang, C. Liu, Z. He, P. Li, W. Zhang, W. Zhang and B. Tang, *Anal. Chem.*, 2021, **93**, 6551–6558.

42 M. Watanabe, S. M. Houten, C. Mataki, M. A. Christoffolete, B. W. Kim, H. Sato, N. Messaddeq, J. W. Harney, O. Ezaki, T. Kodama, K. Schoonjans, A. C. Bianco and J. Auwerx, *Nature*, 2006, **439**, 484–489.

43 G. A. Kullak-Ublick, B. Stieger and P. J. Meier, *Gastroenterology*, 2004, **126**, 322–342.

44 B. Hagenbuch and C. Gui, *Xenobiotica*, 2008, **38**, 778–801.

45 D. Q. Chen, X. Wang, L. Chen, J. X. He, Z. H. Miao and J. K. Shen, *Acta Pharmacol. Sin.*, 2011, **32**, 664–672.

46 F. Holzinger, C. D. Schteingart, H.-T. Ton-Nu, C. Cerrè, J. H. Steinbach, H.-Z. Yeh and A. F. Hofmann, *Hepatology*, 1998, **28**, 510–520.

47 Y. Wu, L. Sun, F. Zeng and S. Wu, *Photoacoustics*, 2019, **13**, 6–17.

48 Z. Luo, Z. Huang, K. Li, Y. Sun, J. Lin, D. Ye and H.-Y. Chen, *Anal. Chem.*, 2018, **90**, 2875–2883.

49 R. Yang, S. Zhang, A. Cotoia, N. Oksala, S. Zhu and J. Tenhunen, *BMC Gastroenterol.*, 2012, **12**, 45.

50 A. Ramachandran, M. R. McGill, Y. Xie, H.-M. Ni, W.-X. Ding and H. Jaeschke, *Hepatology*, 2013, **58**, 2099–2108.

51 J. Ghosh, J. Das, P. Manna and P. C. Sil, *Free Radic. Biol. Med.*, 2010, **48**, 535–553.

52 D. Cheng, W. Xu, L. Yuan and X. Zhang, *Anal. Chem.*, 2017, **89**, 7693–7700.

53 X. Jie, M. Wu, H. Yang and W. Wei, *Anal. Chem.*, 2019, **91**, 13174–13182.

54 H. Umezawa, M. Ishizuka, T. Aoyagi and T. Takeuchi, *J. Antibiot.*, 1976, **29**, 857–859.

55 A. J. Hanley, K. Williams, A. Festa, L. E. Wagenknecht, R. B. D'Agostino, J. Kempf, B. Zinman and S. M. Haffner, *Diabetes*, 2004, **53**, 2623–2632.

56 G. Abboud and N. Kaplowitz, *Drug Saf.*, 2007, **30**, 277–294.

57 P. Cheng, Q. Miao, J. Li, J. Huang, C. Xie and K. Pu, *J. Am. Chem. Soc.*, 2019, **141**, 10581–10584.

58 W. Zhang, L. Chen, H. Feng, W. Wang, Y. Cai, F. Qi, X. Tao, J. Liu, Y. Shen, X. Ren, X. Chen, J. Xu and Y. Shen, *Free Radic. Biol. Med.*, 2017, **112**, 24–35.

59 J. H. Kim, W. S. Nam, S. J. Kim, O. K. Kwon, E. J. Seung, J. J. Jo, R. Shresha, T. H. Lee, T. W. Jeon, S. H. Ki, H. S. Lee and S. Lee, *Int. J. Mol. Sci.*, 2017, **18**, 1417.

60 P. Wang, Y. Yang, G. Pang, C. Zhang, C. Wei, X. Tao, J. Liu, J. Xu, W. Zhang and Y. Shen, *Free Radic. Biol. Med.*, 2021, **162**, 283–297.